Thermal Impedance and Dynamics of Phase Change Materials under Pulse Train Heating

J.C. Lago
Material Science and Engineering
Texas A&M University
College Station, TX, USA
jclago@tamu.edu

V. Gonzalez Fernandez
Material Science and Engineering
Texas A&M University
College Station, TX, USA
veronicacgf@tamu.edu

M.T. Barako
NG Next Basic Research Laboratory
Northrop Grumman Corp.
Redondo Beach, CA, USA
Michael.Barako@ngc.com

P.J. Shamberger
Material Science and Engineering
Texas A&M University
College Station, TX, USA
patrick.shamberger@tamu.edu

***Abstract*—Phase change materials (PCMs) are excellent candidates for the thermal management of high-power pulsed electronic systems due to their high latent heat of fusion and ability to transform reversibly, but they are often limited by the rate at which they can absorb transient heat. By combining PCMs with high thermal conductivity matrices (e.g., copper foams of sufficiently small pore size), an effective composite slab with the favorable attributes of each component forms. While such composites are theoretically promising, the dynamics of the transient heat transfer process of such a PCM composite under high power pulses remains unclear and demands investigation. Numerical models have previously revealed an anti-resonance zone corresponding to a region of maximal buffering of the transient temperature rise, which depends on thermal conductivity, heat capacity, latent heat of fusion, and geometric factors, including the thickness of the slab. However, experimentally identifying frequencies at which a composite PCM layer buffers a temperature rise and the extent to which it does so remains challenging in materials with nonlinear thermal responses. Here, we develop a contact thermal characterization technique to investigate the dynamic response of a composite PCM slab that undergoes pulsed heating on one side and a quasi-constant temperature boundary condition on the other. We capture the depression in the temperature signal near a heated surface, representing the heat transfer surface of an electronic device or component. The outcomes of the experimental technique provide insights into the thermal impedance of the composite and the underlying thermophysical properties related to absorbing and transferring heat optimally.**

Keywords—PCM/Foam Composite, Thermal Impedance, Thermal Conductivity

I. NOMENCLATURE

Roman

T	temperature, °C
V	voltage, V
P	power, W
R	thermal resistance, $°C \cdot W^{-1}$
h	heat transfer coefficient, $W \cdot m^{-2} \cdot °C^{-1}$
L	latent heat of fusion, $J \cdot g^{-1}$
Z	thermal impedance, $°C \cdot W^{-1}$
t	time, s
DF	duty factor, unitless
f	frequency, s^{-1}
A	area, m^2
$\dot{q}$	heat rate, W
q''	heat flux, $W \cdot m^{-2}$
p	period, s

Greek

κ	thermal conductivity, $W \cdot m^{-1} \cdot °C^{-1}$
ρ	density, $g \cdot cm^{-3}$
ϕ	porosity, %
δ	thickness, m

Subscripts

hot	hot
cold	cold
ambient	ambient
melt	melting
on	on
off	off
th	thermal
eff	effective
in	input
interface	interface
baseline	baseline
undercooling	undercooling

Acronyms

PPI	pores per inch
FOM	figure of merit
PCM	phase change material
DAQ	data acquisition
SS	stainless steel

II. INTRODUCTION

Phase change materials (PCMs) are excellent candidates for energy storage and cooling applications due to their ability to absorb heat during an endothermic reaction associated with a structural phase transformation [1]–[4]. These materials have high gravimetric ($J \cdot g^{-1}$) and volumetric ($J \cdot m^{-3}$) energy densities that transform with a high degree of reversibility during

operation. As an example, paraffins (C_nH_{2n+2}) have an enthalpy of fusion that reaches (200 to 225) $J \cdot g^{-1}$ [5], thermal stability displaying a 1.8% drop in latent heat after 900 cycles [6], and tailorable melting temperatures via chemical compositions [7]. However, PCMs generally have low intrinsic thermal conductivity. In the case of paraffins, the thermal conductivity of n-hexadecane ranges from (78 to 143) $mW \cdot m^{-1} \cdot °C^{-1}$ [8], [9]. Low thermal conductivity values decrease the heat transfer rates of PCMs, resulting in larger temperature rises at the heated surface during melting, thus hindering PCMs from widespread adoption. For this reason, PCM composites consisting of closely spaced PCMs and highly thermally conductive materials (e.g., PCM-filled metal foams or lamellar composites) have attracted much interest due to their ability to introduce a tunable mix of high thermal conductivity with high thermal energy storage capacity [10]–[13].

PCM composites integrated into electronic packages can serve as cooling components by providing thermal buffering near chip junctions [14], [15]. Applications for this technology are wide: GaN power transistors [16], SiC-based devices [17], diode arrays and solid-state lasers [18], NiTiHf thermal energy storage (TES) devices [19], and electric vehicle batteries [20]. Traditionally, cooling packages include a combination of liquid or air heat sinks to reject heat to a surrounding fluid, or heat pipes or other heat spreaders to transport heat away from a junction, and are designed to minimize steady state temperature rise. However, in the case of intermittent high-power density systems, integrating PCM composites into an electronics package has the potential to reduce the overall size of cooling packages by absorbing transient pulses of heat, thereby reducing the size of the peak heat load which the heat sink is designed to dissipate.

Composites can comprise various PCMs, including organic waxes, inorganic liquid metals, shape memory alloys, and salt hydrates as PCMs [2], [21]. A distinction among these options is the wide selection of latent heat of fusion quantities and differing melting temperatures [5]. On the other hand, the connected matrices (e.g., foams/honeycombs) can consist of any highly thermally conductive material (e.g., copper, aluminum, or graphite) that is, ideally, connected thermally with limited tortuosity in the primary direction of heat flow. Considerations in the selection of conductive matrices include geometry, dimensions, volume fraction, and, in the case of foams, porosity (%) and pores per inch (PPI) [22].

Different combinations of the PCM and the thermally conductive matrix material result in trade-offs in the composite PCM's effective thermal conductivity and energy storage capability. For example, SABPA/paraffin/EG-DBN composites reach a high thermal conductivity of 7.2 $W \cdot m^{-1} \cdot °C^{-1}$ with a latent heat of fusion of 93.5 $J \cdot g^{-1}$ [23]. This represents an increase of 50× in thermal conductivity and a decrease of 2.4× in the latent heat of fusion when compared to hexadecane. Similarly, paraffin/copper foam composites have reached conductivities of (3.1 to 3.8 $W \cdot m^{-1} \cdot °C^{-1}$). However, with conductivities greater than 5 $W \cdot m^{-1} \cdot °C^{-1}$[24], [25], these composites show diminishing returns due to decreasing latent heat of fusions and PCM volume fractions. In this study, metal open-cell foams with paraffin waxes were utilized (e.g., hexadecane/copper foam), providing a simple and cost-effective means to increase thermal conductivity.

The development of experimental instrumentation to measure thermal impedance in PCM composites is needed to evaluate their efficacy as a thermal management tool for electronics packages. Specifically, transient thermal characterization is required 1) to evaluate what conditions result in thermal buffering under dynamic heating boundary conditions and 2) to validate modeling theories, including assumptions about the role of interfacial phenomena and the impact of thermal heterogeneities in PCM composites. Such novel instrumentation requires the characterization of dynamic heating profiles with well-defined boundary conditions, melt-front dynamics, and thermophysical properties, including undercooling. The challenge here lies in experimentally characterizing a dynamic thermal response comparable to theoretically predicted behaviors [1]. We anticipate this response to differ from an individual heating step function, as the observed thermal response contains kinetic limitations attributable to both the heating (melting) and the cooling (solidifying) contributions. Currently, literature shows that most instrumentation focuses on constant power signals and static temperature profiles to measure thermal conductivities and linear thermal responses [23]–[25]. More recently, we have developed a quasi-one-dimensional dynamic characterization technique implementing harmonic or pulse-train heat flux boundary on one surface of a slab and a convective cooling boundary condition on the opposing surface. This technique was used to evaluate slabs of octadecane and T-304 annealed stainless steel [15]. The experimental rig swept both frequency and power amplitudes to determine the thermal response of the PCM slab. In an associated numerical study, we revealed an anti-resonance zone in which specific frequency and power amplitudes can maximize the buffering of temperature profiles [26]. In this zone, the optimal conditions led to a continuous melt-solidification transition throughout the entire PCM slab, maximizing utilization.

This study further develops the experimental characterization protocol and the physical setup described above by incorporating new instrumentation capabilities (e.g., pulse train heating), with the primary goal being the characterization of thermal impedance in a slab. Herein, we describe the methodology and procedures for using the dynamic experimental rig and include results from data collection of a model PCM slab as an example. We utilize hexadecane impregnated in copper foams with an aggregate thermal conductivity of 1.5 $W \cdot m^{-1} \cdot °C^{-1}$. Based on this data, we present thermal impedance plots for copper foams with and without PCM. This study has three primary outcomes: 1) an optimized experimental setup that minimizes parasitic losses and interfacial resistances, 2) a demonstration of this setup on determining the thermal impedance of a copper foam serving as a linear resistor, and 3) an initial implementation of the dynamic response of a paraffin/copper foam composite.

III. Methods

A. Material Selection

The metallic matrices chosen include 4.08 cm and 2.58 cm thick T-304 stainless steel (SS) blocks and 1.07 cm thick as-received copper foam with a 96.7% porosity (ϕ) and 29.7 pores per inch (PPI). All samples had dimensions of 2.44 cm in length and width. The PCM material chosen was 99% pure hexadecane (Sigma-Aldrich) with a melting point (T_{melt}) of 17.9 °C and a latent heat of fusion (L) of 225.3 $J \cdot g^{-1}$ measured using a TA Q2000 Differential Scanning Calorimeter (DSC) at a heating rate of 2 $°C \cdot min^{-1}$.

B. Experimental Setup and Sample Preparation

The dynamic system consists of a quasi-one-dimensional system with a heat flux boundary applied by a thick film heater on an insulated (quasi-adiabatic) top surface (Fig. 1). The heat flux boundary condition is regulated by a 31.8 W DC power supply (Keysight B2961A) controlling the power applied by a thick film polyimide heater (Omega Heater KHLVA-101/10). On the bottom surface is a quasi-isothermal cooling boundary condition controlled by a mini-channel cold plate (Advanced Thermal Solutions ATS-CP-1002; 0.005 $°C \cdot W^{-1}$ at 4 $L \cdot min^{-1}$). This cold plate is connected to a water chiller (PolyScience LS51M11A110C) (Fig. 1) with a T_{cold} of 10, 15, or 25 °C. The data acquisition (DAQ) system consisted of a National Instruments DAQ-9174 combined with a TB-9212 Isothermal Terminal Block and a 9252 Voltage Input Block.

Three fine-wire K-type thermocouples (Omega 5SC-TT-K-40-36-ROHS) are used to collect temperature data. One thermocouple is placed beneath the heater (T_{hot}), one is fixed to the cold plate (T_{cold}) next to the sample to avoid adding additional thermal resistance (R) to the cold plate/sample interface, and one is outside the system measuring ambient temperature ($T_{ambient}$). Polyimide tape is used to fix the thermocouple on the cold plate, and fiberglass insulation is placed on top for insulation. The thermocouples are calibrated to within 0.1 °C to ensure data accuracy.

This experiment was critical to achieving reasonable repeatability and accuracy, especially across sample-heater and sample-cold plate interfaces. Each sample was prepared with layers to enhance one-dimensional heat transfer and reduce interfacial resistances ($R_{interface}$). Because of the copper foam's topology, the thermal conduction path at the surface with the heater and the cold plate is inhibited by a low contact surface area due to the foam's ligaments. Therefore, a layer of aluminum foil was used as a heat spreader and was fixed by silver conductive epoxy (EPO-TEK® H20E; 2.5 $W \cdot m^{-1} \cdot °C^{-1}$ from laser flash analysis (LFA) and 29 $W \cdot m^{-1} \cdot °C^{-1}$ from thermal resistance data) at the interface between the heater and the sample and the cold plate and the sample. Approximately 0.6 g of silver epoxy was applied at each interface to ensure the metal foam struts had sufficient thermal contact with the foil.

An acrylonitrile butadiene styrene (ABS) sample holder fabricated using a Stratasys F370 printer is fixed to the cold plate with silicone adhesive to contain liquid PCM and to reduce heat loss to the environment. To mount the sample onto the insulating holder, 0.3 g of thermal paste was applied to the sample's bottom interface using a quincunx pattern. In addition, to prevent PCM and silver thermal paste (Arctic Silver 5 AS5-3.5G; 8.9 $W \cdot m^{-1} \cdot °C^{-1}$) contamination, the heater was attached to the sample/foil by adding a layer of silver conductive epoxy. The high-temperature hot-melt adhesive was applied around the sample's bottom edges to shield the paste from mixing with the PCM.

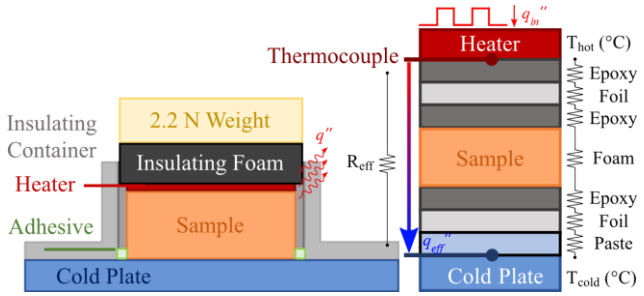

Fig. 1. *On the left is an experimental rig designed to capture dynamic and static responses of PCM slabs. On the right is an exploded view depicting a linear thermal resistance model during constant heating.*

An insulating silicone open-cell foam wrapped in polyimide tape was placed on top of the sample to reduce heat loss from the top surface. To minimize thermal contact resistances associated with the various interfaces, a 2.2 N weight is placed on top to provide a consistent compressive force across all experiments.

C. Data Collection and Processing

A LabVIEW program was written to control the power supply and record temperature and voltage readings from the setup. Two testing modes were used: stepwise and pulse train power inputs. Temperatures and voltages were recorded at a sampling rate of 300 Hz. The duration of each run varied depending on the testing mode to allow the system to reach a steady state. For the stepwise runs, the power varied from 0 to 5 W. For the pulse trains, a constant power of 2.6 W was applied using a 0 V lower level and a 14 V peak level input with a 75.4-ohm resistance from the polyimide heater. For each run, the heater applies a pulsed thermal input, where the pulse train's duty factors (DF) and on times (t_{on}) are an array input to the program.

Temperature profiles (T_{hot}, T_{cold}, and $T_{ambient}$) were collected for each sample and analyzed using MATLAB. For the stepwise case, the temperature rise is measured using the difference between the steady-state, hot-side temperature at each power level and cold-side temperature. For the pulse train case, the periodic unsteady thermal response is allowed to reach sufficient cycles to reach a convergent periodic thermal response at each combination of duty factor and on-time. A script was used to identify the maximum temperature rise for the last 30% of the collected convergent periodic responses. The reported hot-side temperature (T_{hot}) is the mean value of the last 30% peaks. The collected $T_{ambient}$ measured during each experiment was observed to cause small deviations between the runs.

IV. RESULTS AND DISCUSSION

The experimental rig and DAQ system described above and shown in Fig. 1 can measure 1) the steady-state thermal resistance and the thermal impedance of PCM/foam composites across a desired range of frequencies (100 µHz to 50 Hz) and 2) the behavior of undercooling phenomena in the time-dependent and periodic temperature profiles. This study concludes with a discussion of how pulse-train heating and degrees of undercooling affect the performance of PCM composites for the thermal management of electronic packages.

A. Instrumentation Methodology and Procedures

The experimental rig was designed to determine a composite slab's thermal impedances and resistances in a complex design space. The rig can probe a hypercube parameter space of heat fluxes, cold-side temperatures, duty factors, on-times, material systems, and slab thicknesses. However, to simplify the parameter space, we focused on a heat flux q'' of 0.433 W·cm^{-2} (corresponding to 2.6 W), three cold-side temperatures, duty factors of (0.01 to 0.5), and on-times of (0.01 to 100) s. The three cold-side temperatures chosen were 10, 15, and 25°C, representing a temperature below, near, and above hexadecane's melting point (T_{melt} = 17.9 °C). A 1.07 cm thick copper foam infiltrated with hexadecane was used in this study.

The thermal response was characterized in three different ways, as shown in Fig. 2: 1) steady-state conditions to characterize the total effective resistance and interfacial resistances, 2) step-change heating as the idealized low-frequency (DF = 0) and low impedance response, and 3) periodic pulse train heating with different DF and t_{on}. The three types of characterizations are listed in order of operation. First, the steady-state response was analyzed to minimize the system's interfacial resistances. Then, the step-change response determines the lowest and highest on-times needed for the transient-state method. Finally, the transient-state response probes the slab's performance in buffering temperature profiles as a function of frequency.

The goal of the steady-state measurement is to identify and minimize parasitic losses and interfacial resistances that can later impact the dynamic response. In addition, by reducing interfacial resistances, the setup avoids additional characteristic dynamic times. The issue of interfacial resistances is particularly critical given the concern of distortion of foam struts which could result in poor thermal contact at the interfaces with the cold plate and the heated surface. Therefore, to reduce these interfacial resistances, an aluminum foil was epoxied onto the top and bottom surface of the foam to serve as a heat spreader, the heater was epoxied on top, and thermal paste was added at the bottom, as shown in Fig. 1.

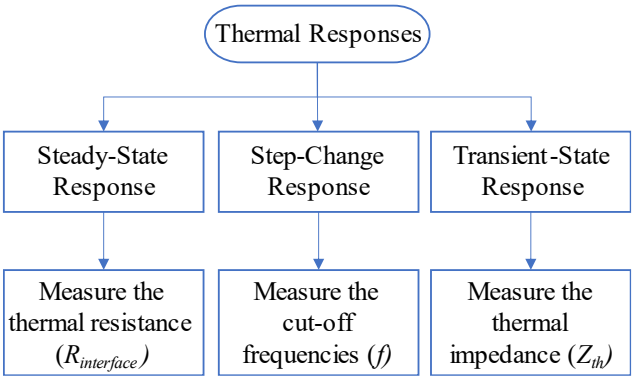

Fig. 2. *Process flow map culminating the results of the experimental methodology for the dynamic PCM/foam characterization instrument.*

B. Steady State Characterization Method

The steady-state response in Fig. 3 measures the aggregate thermal resistances and the conditions needed to characterize the interfacial sample resistances. The linear model, as shown in Fig. 1, comprises the following resistors in the epoxy, foil, sample, and thermal paste components:

$$R_{eff} = R_{epoxy,\ foil,\ epoxy} + R_{sample} + \mathrm{R}_{\mathrm{epoxy,\ foil,\ paste}} \quad (1)$$

The resistances in equation (1) represent an effective thermal resistance across the copper foam slab. In this system, the interfacial resistance ($R_{interface}$) is the summation of the epoxy, foil, and paste components. To calculate the interfacial contribution, we use a SS slab with a known thermal conductivity of 14.4 W·m^{-1}·°C^{-1} [27] to back-calculate the sample's thermal resistance. Several sample preparation iterations were used to minimize the interfacial resistances.

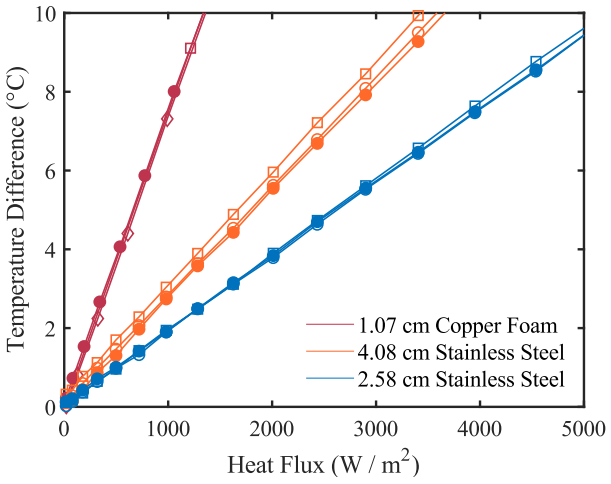

Fig. 3. *The temperature difference between the hot-side and the cold-side temperatures at constant power. Red is the foam, orange is the 4.08 cm SS, and blue is the 2.58 cm. Solid circles, open circles, squares, and diamonds are the cold-side temperatures at 25, 20, 15, and 10 °C.*

Measuring the steady-state response consists of a polyimide heater that sweeps through a series of constant power values. First, the system reaches a steady-state temperature at each

power level. Then, a MATLAB script takes the temperature difference between the steady-state hot-side and cold-side temperatures. Fig. 3 shows the steady-state response for the 1.07 cm thick copper foam, the 4.08 cm thick SS, and the 2.58 cm thick SS at all three cold-side temperatures.

Fourier's law and Newton's law of cooling ($\dot{q} = \kappa A_{cross\text{-}section} \Delta T / \delta$; $\dot{q} = h A_{surface} \Delta T$) are used in measuring the system's thermal resistances. In addition, the power input ($\dot{q}_{in}$) was related to the conduction through the slab ($\dot{q}_{eff}$) and convective cooling losses to ambient air ($\dot{q}_{ambient}$). Thus, energy balance considerations result in the following:

$$\dot{q}_{in} = \dot{q}_{eff} + \dot{q}_{ambient} \tag{2}$$

$$P = \frac{T_{hot} - T_{cold}}{R_{eff}} + h A_{sa} (T_{hot} - T_{ambient}) \tag{3}$$

Equation (3) uses the effective thermal resistance (R_{eff}) from equation (1) and serves as the fitting function to the experimental data in Fig. 3. We use a nonlinear regressor to calculate the interfacial resistance using the known thermal conductivity from the SS slabs. Then, the thermal conductivity of the copper foam can be back-calculated using the interfacial resistance and convective losses calculated from the SS slab ($\kappa_{sample} = (R_{eff} - R_{interface})(\delta / A_{ca})$). Table I shows the resulting κ, h, $R_{interface}$, and R_{sample} values. The thermal conductivity of the copper foam was 1.49 $W \cdot m^{-1} \cdot °C^{-1}$ with an associated thermal resistance of 12.0 $°C \cdot W^{-1}$. Overall, the outcome showed an interfacial resistance of 2.33% to the foam's thermal resistance.

TABLE I. STEADY-STATE PARAMETERS

Material	κ $(W \cdot m^{-1} \cdot °C^{-1})$	h $(W \cdot m^{-2} \cdot °C^{-1})$	$R_{interface}$ $(°C \cdot W^{-1})$	R_{sample} $(°C \cdot W^{-1})$
Stainless Steel	14.4	3.64	0.33	3.92
	14.4	1.08	0.22	2.31
Copper Foam	1.49	2.36	0.28	12.0

C. Unsteady Periodic Heating

The experimental rig can operate using a pulse train heating boundary that sweeps a sequence of *DF*s and t_{on}, simulating an electronics-heated surface. In this method, the power signal is a pulse train represented by a ratio of on-times (t_{on}) to a period (p). Duty factors (*DF*), on-times, and frequency (f) relate according to the following equations:

$$DF = \frac{t_{on}}{t_{on} + t_{off}} = \frac{t_{on}}{p} \tag{4}$$

$$f = \frac{1}{p} = \frac{DF}{t_{on}} \tag{5}$$

A LABVIEW script utilizes equation (4) to sweep through an array of *DF* and t_{on}. A fixed timer is used as a stop criterion for each combination of *DF* and t_{on}. We account for the nearly 10 min settling time in the lower *DF* in Fig. 4 by allowing the response sufficient time to converge. On the other hand, to measure the idealized (*DF* = 0) single pulse response, the step-change method cycles a range of on-times with a fixed off-time.

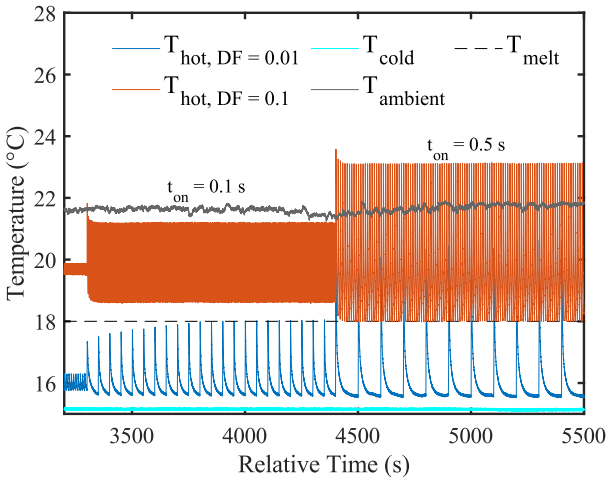

Fig. 4. *A temperature profile of the transient thermal response of an empty copper foam. Orange is a DF of 0.1, and blue is a DF of 0.01. The ambient, cold-side, and melting temperatures are the grey, light blue, and dashed lines.*

In Fig. 4, a schematic shows a typical transient-state response. For simplicity, the plot uses relative time in the x-axis to represent a time change from start to finish. It shows a *DF* sweep from 0.01 to 0.1 and an on-time sweep from 0.1 to 0.5 s. Only a small portion of the complete data set is shown for brevity, and the 0.1 *DF* curve (orange) was laid on top for comparison.

For the case of the copper foam without PCM, the frequency-dependence of the transient response is highly repeatable across cycles, as shown in Fig. 4. In general, the temperature profile is greater at larger *DF*s when compared to smaller *DF*s at the same on-times. Additionally, the quasi-steady state temperature increases as on-times increase within a single *DF*. This duty factor and on-time effect are further confirmed by measuring the system-level thermal impedance.

D. Thermal Impedance of Empty Copper Foams

The thermal performance of PCM composites as heat sinks coupled with thermal capacitors relies on their ability to draw heat out of a surface. Therefore, thermal impedance calculations are a valuable way to visualize the frequency-dependent system-level thermal resistances normalized by power. For the case of copper foam, a prototypical impedance curve is developed using the following relation:

$$Z_{th,\,DF} = \frac{\max(T_{hot}) - T_{hot,\,baseline}}{P} \tag{6}$$

At a single *DF* and power (P), the impedance is a sequence of values at each on-time making up the curves seen in Fig. 5. The maxima of T_{hot}, $\max(T_{hot})$, was measured for each heating pulse, as shown in Fig. 4. For a particular combination of *DF* and t_{on}, $\max(T_{hot})$, used to calculate Z_{th}, was the average of the last 30% of the peaks collected under a set of conditions, to

allow the system thermal response to converge to quasi-steady state behavior. To calculate thermal impedance, the hot-side baseline temperature, $T_{hot,\ baseline}$, was collected with no heating applied after the system had achieved thermal steady-state with the cold heat sink at a particular T_{cold}.

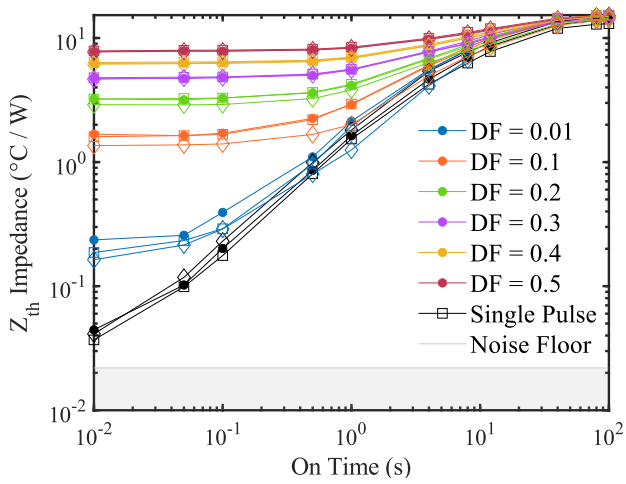

Fig. 5. *The thermal impedance of the copper foam composite for DF 0.01 to 0.5 and on-times 0.01 to 100 s. Diamonds are a cold-side temperature of 10 °C, squares of 15 °C, and solid circles of 25 °C. Colors black to red represent DFs, as shown in the legend, and the grey-shaded region is the noise level.*

For the case of the empty copper foam (without PCM), thermal impedance curves are independent of T_{cold} and behave as linear thermal resistors. Additionally, the grey line in Fig. 5 represents a noise level of 0.01 °C·W^{-1}, which limits the lowest impedance that can be measured with the present system. The noise was measured by using the two-sigma standard deviation of the quasi-steady state at the lowest *DF* of 0.01 and an on-time of 0.01 s.

At long and short on-times, impedances converge as quasi-steady states are reached. At long on-times, the impedance converges by an on-time of 100 s across all *DF*s as the system reaches a quasi-steady state at a power of 2.6 W. On the other hand, at short on-times, the system converges at a quasi-steady state related to the time-averaged heating power, as the system does not have time to fully relax during t_{off}. Also, for the linear case, impedance tends to increase as on-time increases. Similarly, it was observed that the impedance increases as DF increases. Overall, the single pulses had the lowest impedance value of 0.04 °C·W^{-1} at an on-time of 0.01 s, while the highest impedance value was 15.3 °C·W^{-1} at an on-time of 100 s.

E. Undercooling Effect in PCM Composites

The challenge to characterizing nonlinear PCM elements for thermal management applications includes open questions on the effects that transient-state heating has on transition dynamics and thermal performance [16]–[20]. For example, different amounts of phase fraction transform at various *DF*s and on-times depending on the heating and cooling rates. On top of that, the solidification fronts are impacted and inhibited by undercooling [28], [29]. During the solidification, the transition evidenced a nucleation-limited undercooling phenomenon.

Hexadecane is a paraffin PCM [4] that buffers the temperature of a heated surface and suffers from minor supercooling. However, the presence of undercooling effects can be easily overlooked in thermal impedance curves. Therefore, instrumentation requires components with the sensitivity to capture undercooling in the temperature profiles and, ultimately, in the thermal impedance plots.

Fig. 6 a) depicts the outcome of thermal buffering as a function of *DF*s from 0.1 to 0.17 and on-times from 2.5 to 10 s. In the temperature profiles in Fig. 6 a), the PCM melts and solidifies, as shown by the dashed line melt (T_{melt}). However, at a *DF* of 0.17 and an on-time of 7.5 s, the temperature is additionally buffered by a total of 0.57 °C compared to the equivalent peaks at the *DF* of 0.1. Similarly, at the on-time of 10 s, the temperature has buffered a total of 2.05 °C, suggesting a temperature dependence on *DF* and t_{on}.

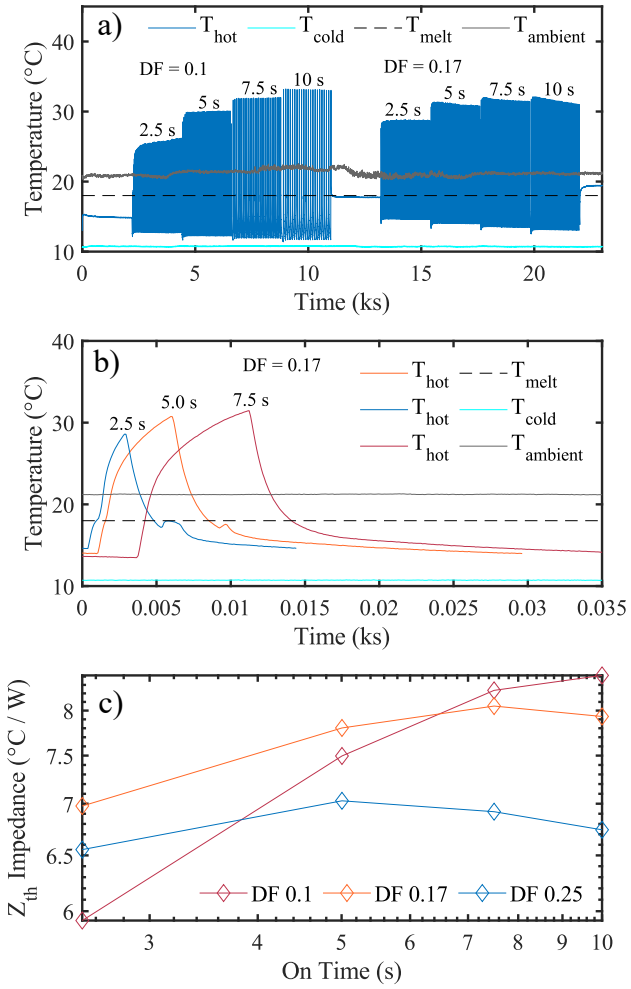

Fig. 6. *Thermal response of the PCM/foam composite at DFs 0.1 to 0.25 and on-times 2.5 to 10 s. (a) The temperature profile of the hot-side, cold-side, and ambient temperatures at various DFs and on-times. (b) The individual pulses at a DF of 0.17 and an on-time of 2.5, 5.0, and 7.5 s. (c) The thermal impedance derived from the data in (a).*

A closer look at the individual temperature peaks of the data in Fig. 6 a) reveals the existence of significant undercooling by the presence of secondary peaks. For example, in Fig. 6 b), at a

DF of 0.17, the secondary peak at a t_{on} of 2.5 s reaches an amplitude of 0.79 °C. Then, a peak amplitude of 0.45 °C occurs at a t_{on} of 5.0 s. However, by 7.5 s, the undercooling phenomena are indiscernible and highly diminished. Similarly, consistent secondary peaks were observed at a lower *DF* of 0.1 but diminished at a higher *DF* of 0.25.

The thermal impedances in Fig. 6 c) overall reflect a *DF* of 0.25 with the lowest impedance of 6.7 °C·W^{-1} at a t_{on} of 10 s. On the other hand, the *DF* of 0.1 has the highest impedance of 8.4 °C·W^{-1} at the t_{on} of 10 s. The plot reflects additional thermal buffering as the on-time increases from 5 to 10 s in the *DFs* of 0.17 and 0.25. For example, at the *DF* of 0.17, the impedance drops by 1.5% during the on-times of 7.5 s to 10 s. At the *DF* of 0.25, a drop of 4.1% occurs, signifying additional temperature buffering at the higher *DF*. Similarly, the *DF*s of 0.17 and 0.25 have lower impedances than the *DF* of 0.1 at specific crossover points, which also indicates the buffering effect. Because the material's thermal conductivity, latent heat of fusion, and the applied heat flux do not change for the PCM/foam composite during the experiment, the reduction in impedance is attributed to a frequency-dependence phenomenon correlating melt fraction and undercooling degrees to better PCM utilization.

Undercooling plays a role in the regime of *DF*s and on-times that can optimally buffer temperature. For example, the responsivity of the PCM composite at a *DF* of 0.17 and a t_{on} of 7.5 s was observed, where the secondary peaks diminish entirely after a few cycles. Then, at a *DF* of 0.2, with a greater buffering, secondary peaks are absent across all t_{on}. The observations imply that 1) thermal buffering optimization occurs at specific *DF*s and t_{on} due to greater PCM utilization and 2) undercooling peaks diminish at specific frequency regimes. These outcomes testify to the instrument's capability of capturing nonlinear and transient information and merit a systemic study of the operational regime and undercooling effects, which can lead to optimal buffering.

V. Conclusions

PCM composites represent nonlinear capacitive elements for electronic packages, which may serve as transient heat sinks for pulsed, unsteady heat loads. However, it remains unclear over what frequency range these elements can effectively serve to buffer temperature rise for an electronics package. For very high frequencies, there is insufficient time for heat to transfer into a composite PCM. For very low frequencies, the entire PCM melts, after which it is no longer able to store heat. To resolve these questions, we develop a novel instrumentation device to characterize a PCM composite's steady-state and transient-state dynamic heating at varying cold-side temperatures. Overall, a prototype of the instrument's capabilities is presented using hexadecane/copper foam composites under duty factors of (0 to 0.5) and on-times of (0.01 to 100 s). The resulting thermal impedance characterization reveals thermal buffering at specific duty factors and on-times. At the optimal conditions, undercooling peaks disappeared at the *DF*s of 0.17 and 0.25 and on-times of 7.5 s and 10.0 s. Overall, the lower thermal impedance observed is attributed to better PCM utilization at specified frequencies, which is related to optimal melt fractions and degrees of undercooling.

The instrument methodology describes a procedure to sequentially measure 1) the steady-state sample thermal resistance and interfacial resistance, 2) the cut-off frequencies below which the composite PCM absorbs negligible heat, and 3) the overall thermal impedance relations. A step-by-step process covers the steps to characterizing an example composite PCM sample under the steady-state, step-change, and transient-state methods. First, the steady-state method measured a thermal conductivity of 1.49 W·m^{-1}·°C^{-1} and an interfacial resistance of 0.28 °C·W^{-1} for the copper foam. Then, the thermal impedance for the copper foam filled with PCM was measured using the transient characterization method. The general trend in the copper foam reveals an increasing thermal impedance with increasing duty factors and on-times. However, with the addition of hexadecane, the system observed additional temperature buffering at specific duty factors and on-times. In the future, this technique will be applied to a variety of composite PCM structures to evaluate the role of geometric dimensions, critical composite length scales, and intrinsic material properties on a sample's thermal impedance.

References

[1] P. J. Shamberger, "Mapping design trade-offs," *Nat Energy*, vol. 6, no. 3, Art. no. 3, Mar. 2021, doi: 10.1038/s41560-021-00803-y.

[2] L. F. Cabeza, A. Castell, C. Barreneche, A. de Gracia, and A. I. Fernández, "Materials used as PCM in thermal energy storage in buildings: A review," *Renewable and Sustainable Energy Reviews*, vol. 15, no. 3, pp. 1675–1695, Apr. 2011, doi: 10.1016/j.rser.2010.11.018.

[3] T. Nomura, N. Okinaka, and T. Akiyama, "Impregnation of porous material with phase change material for thermal energy storage," *Materials Chemistry and Physics*, vol. 115, no. 2, pp. 846–850, Jun. 2009, doi: 10.1016/j.matchemphys.2009.02.045.

[4] K. Yazawa, P. J. Shamberger, and T. S. Fisher, "Ragone Relations for Thermal Energy Storage Technologies," *Frontiers in Mechanical Engineering*, vol. 5, 2019, doi: https://doi.org/10.3389/fmech.2019.0002.

[5] S. Ahmed, A. Hoe, F. Alamo, N. Turner, and P. J. Shamberger, "Experimental determination of high energy density lithium nitrate hydrate eutectics," *Journal of Energy Storage*, vol. 52, p. 104754, Aug. 2022, doi: 10.1016/j.est.2022.104754.

[6] G. Ferrer, A. Solé, C. Barreneche, I. Martorell, and L. F. Cabeza, "Review on the methodology used in thermal stability characterization of phase change materials," *Renewable and Sustainable Energy Reviews*, vol. 50, pp. 665–685, Oct. 2015, doi: 10.1016/j.rser.2015.04.187.

[7] C. Vélez, M. Khayet, and J. M. Ortiz de Zárate, "Temperature-dependent thermal properties of solid/liquid phase change even-numbered n-alkanes: n-Hexadecane, n-octadecane and n-eicosane," *Applied Energy*, vol. 143, pp. 383–394, Apr. 2015, doi: 10.1016/j.apenergy.2015.01.054.

[8] M. J. Assael, E. Charitidou, and L. Karagiannidis, "The thermal conductivity of n-hexadecane+ ethanol and n-decane+butanol mixtures," *Int J Thermophys*, vol. 12, no. 3, pp. 491–500, May 1991, doi: 10.1007/BF00502364.

[9] S. A. Monogenidou, M. J. Assael, and M. L. Huber, "Reference Correlation for the Thermal Conductivity of *n* -Hexadecane from the Triple Point to 700 K and up to 50 MPa," *Journal of Physical and Chemical Reference Data*, vol. 47, no. 1, p. 013103, Mar. 2018, doi: 10.1063/1.5021459.

[10] A. R. Hoe, D. Perez-Nunez, J. R. Felts, and P. J. Shamberger, "Numerical evaluation of thermal energy storage rate in planar and cylindrical phase change material composites," *Journal of Energy Storage*, vol. 55, p. 105430, Nov. 2022, doi: 10.1016/j.est.2022.105430.

[11] A. Hoe, A. Easley, M. Deckard, J. Felts, and P. J. Shamberger, "Forward Selection Methodology for Phase Change Material Composite Optimization," in *2020 19th IEEE Intersociety Conference*

on Thermal and Thermomechanical Phenomena in Electronic Systems (ITherm), Jul. 2020, pp. 674–680. doi: 10.1109/ITherm45881.2020.9190188.

[12] A. Hoe *et al.*, "Objective oriented phase change material composite heat sink design," *Applied Thermal Engineering*, vol. 209, p. 118235, Jun. 2022, doi: 10.1016/j.applthermaleng.2022.118235.

[13] A. Hoe, M. Deckard, A. Tamraparni, A. Elwany, J. R. Felts, and P. J. Shamberger, "Conductive heat transfer in lamellar phase change material composites," *Applied Thermal Engineering*, vol. 178, p. 115553, Sep. 2020, doi: 10.1016/j.applthermaleng.2020.115553.

[14] M. Deckard, P. Shamberger, M. Fish, M. Berman, J. Wang, and L. Boteler, "Convergence and Validation in ParaPower: A Design Tool for Phase Change Materials in Electronics Packaging," in *2019 18th IEEE Intersociety Conference on Thermal and Thermomechanical Phenomena in Electronic Systems (ITherm)*, May 2019, pp. 878–885. doi: 10.1109/ITHERM.2019.8757334.

[15] A. Hoe, C. Martinez, M. Barako, and P. J. Shamberger, "Dynamic Characterization of Phase Change Materials Under Harmonic Heating," in *2021 20th IEEE Intersociety Conference on Thermal and Thermomechanical Phenomena in Electronic Systems (iTherm)*, Jun. 2021, pp. 1162–1167. doi: 10.1109/ITherm51669.2021.9503173.

[16] R. S. Pengelly, S. M. Wood, J. W. Milligan, S. T. Sheppard, and W. L. Pribble, "A Review of GaN on SiC High Electron-Mobility Power Transistors and MMICs," *IEEE Transactions on Microwave Theory and Techniques*, vol. 60, no. 6, pp. 1764–1783, Jun. 2012, doi: 10.1109/TMTT.2012.2187535.

[17] V. E. Chelnokov and A. L. Syrkin, "High temperature electronics using SiC: actual situation and unsolved problems," *Materials Science and Engineering: B*, vol. 46, no. 1, pp. 248–253, Apr. 1997, doi: 10.1016/S0921-5107(96)01990-3.

[18] S. A. Payne *et al.*, "Diode arrays, crystals, and thermal management for solid-state lasers," *IEEE Journal of Selected Topics in Quantum Electronics*, vol. 3, no. 1, pp. 71–81, Feb. 1997, doi: 10.1109/2944.585817.

[19] D. J. Sharar, B. F. Donovan, R. J. Warzoha, A. A. Wilson, A. C. Leff, and B. M. Hanrahan, "Solid-state thermal energy storage using reversible martensitic transformations," *Appl. Phys. Lett.*, vol. 114, no. 14, p. 143902, Apr. 2019, doi: 10.1063/1.5087135.

[20] N. R. Jankowski and F. P. McCluskey, "A review of phase change materials for vehicle component thermal buffering," *Applied Energy*, vol. 113, pp. 1525–1561, Jan. 2014, doi: 10.1016/j.apenergy.2013.08.026.

[21] N. Hite *et al.*, "NiTiHf shape memory alloys as phase change thermal storage materials," *Acta Materialia*, vol. 218, p. 117175, Oct. 2021, doi: 10.1016/j.actamat.2021.117175.

[22] J. K. Carson, S. J. Lovatt, D. J. Tanner, and A. C. Cleland, "Thermal conductivity bounds for isotropic, porous materials," *International Journal of Heat and Mass Transfer*, vol. 48, no. 11, pp. 2150–2158, May 2005, doi: 10.1016/j.ijheatmasstransfer.2004.12.032.

[23] W. Lee, M. Seo, and J. Kim, "Ultra-high thermal conductivity and mechanical properties of a paraffin composite as a thermal conductive phase change materials for novel heat management," *Composites Science and Technology*, vol. 220, p. 109282, Mar. 2022, doi: 10.1016/j.compscitech.2022.109282.

[24] S. Thapa, S. Chukwu, A. Khaliq, and L. Weiss, "Fabrication and analysis of small-scale thermal energy storage with conductivity enhancement," *Energy Conversion and Management*, vol. 79, pp. 161–170, Mar. 2014, doi: 10.1016/j.enconman.2013.12.019.

[25] A. Siahpush, J. O'Brien, and J. Crepeau, "Phase Change Heat Transfer Enhancement Using Copper Porous Foam," *Journal of Heat Transfer-transactions of The Asme - J HEAT TRANSFER*, vol. 130, Aug. 2008, doi: 10.1115/1.2928010.

[26] P. J. Shamberger, A. Hoe, M. Deckard, and M. T. Barako, "Dynamics of melting in a slab under harmonic heating and convective cooling boundary conditions," *Journal of Applied Physics*, vol. 128, no. 10, p. 105102, Sep. 2020, doi: 10.1063/5.0016060.

[27] R. S. Graves, T. G. Kollie, D. L. McElroy, and K. E. Gilchrist, "The thermal conductivity of AISI 304L stainless steel," *Int J Thermophys*, vol. 12, no. 2, pp. 409–415, Mar. 1991, doi: 10.1007/BF00500761.

[28] L. Wei and K. Ohsasa, "Supercooling and Solidification Behavior of Phase Change Material," *ISIJ International*, vol. 50, no. 9, pp. 1265–1269, 2010, doi: 10.2355/isijinternational.50.1265.

[29] G. A. Lane, "Phase change materials for energy storage nucleation to prevent supercooling," *Solar Energy Materials and Solar Cells*, vol. 27, no. 2, pp. 135–160, Jul. 1992, doi: 10.1016/0927-0248(92)90116-7.